**Atmospheric
Chemistry
and Physics**

Composition and temporal behavior of ambient ions in the boreal forest

M. Ehn[1], H. Junninen[1], T. Petäjä[1], T. Kurtén[1], V.-M. Kerminen[1,2], S. Schobesberger[1], H. E. Manninen[1], I. K. Ortega[1], H. Vehkamäki[1], M. Kulmala[1], and D. R. Worsnop[1,2,3]

[1]Department of Physics, P.O. Box 64, 00014, University of Helsinki, Finland
[2]Finnish Meteorological Institute, Research and Development, P.O. Box 503, 00101 Helsinki, Finland
[3]Aerodyne Research Inc, Billerica, MA 01821, USA

Abstract. A recently developed atmospheric pressure interface mass spectrometer (APi-TOF) measured the negative and positive ambient ion composition at a boreal forest site. As observed in previous studies, the negative ions were dominated by strong organic and inorganic acids (e.g. malonic, nitric and sulfuric acid), whereas the positive ions consisted of strong bases (e.g. alkyl pyridines and quinolines). Several new ions and clusters of ions were identified based on their exact masses, made possible by the high resolution, mass accuracy and sensitivity of the APi-TOF. Time series correlograms aided in peak identification and assigning the atomic compositions to molecules. Quantum chemical calculations of proton affinities and cluster stabilities were also used to confirm the plausibility of the assignments. Acids in the gas phase are predominantly formed by oxidation in the gas phase, and thus the concentrations are expected to vary strongly between day and night. This was also the case in this study, where the negative ions showed strong diurnal behavior, whereas the daily changes in the positive ions were considerably smaller. A special focus in this work was the changes in the ion distributions occurring during new particle formation events. We found that sulfuric acid, together with its clusters, dominated the negative ion spectrum during these events. The monomer (HSO_4^-) was the largest peak, together with the dimer ($H_2SO_4 \cdot HSO_4^-$) and trimer ($(H_2SO_4)_2 \cdot HSO_4^-$). SO_5^- also tracked HSO_4^- at around 20% of the HSO_4^- concentration at all times. During the strongest events, the tetramer and a cluster with the tetramer and ammonia were also detected. Quantum chemical calculations predict that sulfuric acid clusters containing ammonia are much more stable when neutral, thus the detection of a single ion cluster implies that ammonia can be an important compound in the nucleation process. We also believe to have made the first observations of an organosulfate (glycolic acid sulfate) in the gas phase. This ion, and its cluster with sulfuric acid, correlates with the HSO_4^-, but peaks in the early afternoon, some hours later than HSO_4^- itself. A list of all identified ions is presented in the supplementary material, and also a list of all detected masses not yet identified.

1 Introduction

Ions in the atmosphere are produced mainly by cosmic radiation and radioactive decay (e.g. Harrison and Carslaw, 2003). The primary ions formed in this process, such as N_2^+, O_2^+, O_2^- and H_3O^+, subsequently collide with various trace gases, which may result in charge transfer when energetically favorable. In this way, over time, the charges will be transported, through a series of collisions leading to charge transfer, towards the compounds with the highest (positive charges) and lowest (negative charges) proton affinities. Once an ion collides with an aerosol particle or surface, it is considered to be lost. Thus, the ambient ion distribution obtains a pseudo steady state between ion production, transfer, and loss (e.g. Hõrrak et al., 2008, and references therein).

Formation of new aerosol particles via nucleation of low-volatile trace gases has been observed to take place throughout the atmosphere (Kulmala et al., 2004; Kulmala and Kerminen, 2008). Nucleated particles constitute a globally

Correspondence to: M. Ehn
(mikael.ehn@helsinki.fi)

important source of cloud condensation nuclei, with potentially large implications on the Earth's climate system (Wang and Penner, 2009; Merikanto et al., 2009; Andreae and Rosenfeld, 2008). The contribution of ions to atmospheric nucleation has been studied both theoretically (Kerminen et al., 2007; Yu and Turco, 2001; Kazil and Lovejoy, 2004; Yu et al., 2008) and by using various experimental approaches (Gagné et al., 2009; Eisele et al., 2006; Hõrrak et al., 2003; Mirme et al., 2010; Laakso et al., 2007). While many of these studies are suggestive of a minor contribution of ions to the overall nucleation rate (Kulmala et al., 2007; Kulmala et al., 2010), especially in the lower troposphere, no general consensus on this issue has been received (Enghoff and Svensmark, 2008; Kazil et al., 2008). Regardless of their exact role in atmospheric aerosol formation, ions are expected to provide valuable information on this process, since the trace gases participating in nucleation are very likely to influence the number size distribution and chemical composition of atmospheric small ions.

The concentration and size distribution of ions can be measured with time resolutions of minutes or less by using various kinds of ion spectrometers, such as the Balanced Scanning Mobility Analyzer (BSMA, Tammet, 2006), Air Ion Spectrometer (AIS, Mirme et al., 2007), and Neutral cluster and Air Ion Spectrometer (NAIS, Kulmala et al., 2007; Manninen et al., 2009b). With these instruments, physical characteristics of atmospheric ions have recently been investigated in a number of different environments around the world (e.g. Suni et al., 2008; Vana et al., 2008; Laakso et al., 2008; Manninen et al., 2010). Unfortunately, due to the low mobility resolution associated with ion spectrometers (Asmi et al., 2009), no information on the chemistry of atmospheric ions has been obtained from these studies.

To determine the chemical composition of atmospheric ions, mass spectrometer (MS) techniques need to be employed. The first mass spectrometric measurements of tropospheric ions were performed during the 1980s (Eisele, 1989a, b, and references therein), and the same or similar kind of instruments have been used until the last decade (Eisele et al., 2006). These studies have shown that negative ions below a few hundred atomic mass units are dominated by strong acids, such as sulfuric and nitric acid, and their clusters, whereas positive ions consist of molecules and clusters of ammonia, amines and pyridines. The quadrupole MS is limited in applicability due to close to integer mass resolution, in addition to the long integration times needed to sample the entire ion spectrum. With these instruments, a more specific determination of the chemical composition requires MS-MS operation, where additional information is gained by fragmenting selected ions.

Recently, a new atmospheric pressure interface time-of-flight mass spectrometer (APi-TOF) was developed and tested (Junninen et al., 2010). A time-of-flight MS provides a better mass and time resolution than a quadrupole MS. Thus, Junninen et al. (2010), identified several ions in the ambi-

ent air with high certainty, purely based on their (high resolution) masses and temporal behavior, consistent with the previous characterization with the quadrupole MS methods (Eisele, 1989a, b).

In this study, we have deployed an APi-TOF in Hyytiälä, southern Finland, to measure the composition of ambient ions. The aim was to compare the composition of ions in the boreal forest with existing data available by Eisele (1989a, b) and Junninen et al. (2010), and continue the identification work. With the improved sensitivity, the temporal behavior of the ions could also be studied. A special focus was put on determining the changes in the ion composition during new particle formation events, and how this is related to the initial steps of nucleation and growth.

2 Materials and methods

This study utilized both experimental and theoretical methods in the characterization of the ambient ion chemical composition in a boreal forest environment. A suite of instruments were deployed at SMEAR II in Hyytiälä (Hari and Kulmala, 2005). The station is a rural site, located within the boreal forest, with a large range of basic meteorology, particle and gas phase instruments measuring year-round. The experimental characterization of the ambient ions was conducted as a part of the EUCAARI project (Kulmala et al., 2009; Kerminen et al., 2010) intensive observation period in April–May, 2009. The results presented below were collected over the period 30 April–8 May 2009, starting in negative ion mode, and switching to positive ion measurements on 5 May.

Quantum chemical calculations were performed to aid in the interpretation of the measured ion distributions. Proton affinities and gas phase acidities were calculated for several compounds, providing a measure for the stability of the ions. Although the bulk liquid values for proton affinity and acidity for a certain compound is well known, the gas phase values may differ from these. Additionally, formation free energies of selected molecular clusters were calculated. Specific computational details are presented in the supplementary material.

2.1 Ambient ion chemical composition

An atmospheric pressure interface time-of-flight mass spectrometer (APi-TOF) was used to measure the mass spectrum of ions of both polarities. The instrument is previously described by Junninen et al. (2010), and only a brief description will be given here. The instrument inlet is a critical orifice drawing a sample flow of $0.8 \, 1 \, min^{-1}$, and the aim is to transport all the ions into the TOF to determine their mass per charge (m/Q). This is done by using two guiding quadrupoles and an ion lens assembly, in three separate differentially pumped chambers, leading into the TOF. The

TOF, manufactured by Tofwerk AG in Switzerland, has a resolving power specified to 3000 Th/Th and a mass accuracy <20 ppm in "V mode". The ion flight paths can be set to either single ("V mode") or double ("W mode") reflections, optimizing either for signal (V) or resolution (W). In this study only the V mode was used. We will use the Thompson (Th) as the unit for m/Q, which closely corresponds to the mass unit Dalton (Da) for singly charged ions.

The APi-TOF currently provides mass spectra of ions with a transmission efficiency of 0.1–1% (Junninen et al., 2010) in the range 80–800 Th. Effectively the TOF is a band-pass filter for the ions, where there is a sharp cut-off at low m/Q, a relatively stable transmission in the intermediate m/Q range, and a slow decrease at high m/Q. The position of the sharp drop-off at lower sizes, and the rate of transmission loss at higher masses can to some extent be optimized to allow for better throughput of either the small or large ions. In this work, with a focus on studying new particle formation and growth, the transmission range was optimized for the larger ions, which in practice meant a sharp cut-off at around 70 Th (positive ions) and 80 Th (negative ions), and a transmission drop of at least a factor 10 at 1000 Th (both polarities).

In addition to the internal ion losses, the sampling inlet tubing will also produce (size dependent) losses. The inlet of the APi-TOF consisted of stainless steel tubing, roughly 60 cm in length. The first 45 cm was 10 mm outer diameter (OD) tube with a flow rate of 15 l min^{-1}, followed by 15 cm of 6 mm OD tube with a flow of 6 l min^{-1}. Simulated diffusion losses in the inlet tubing showed a transmission of 25–50% in the mass range 100–1000 Da, assuming laminar flow. The final total detection efficiency of the instrument during this campaign was determined by comparing the total ion counts measured by the APi-TOF and a BSMA (see Sect. 2.2.2). No size dependence was taken into account, as this could not be done reliably enough. The uncertainty of the BSMA is reported to be <20%, and this uncertainty will translate to the reported APi-TOF concentrations.

In the expansion into lower pressure, and during ion-gas collisions in the guiding quadrupoles, weakly bound clusters may fragment. The most likely perturbation of the ions is the loss of clustered water molecules. In a recent comparison between the APi-TOF and two ion mobility instruments, very good agreement from sampled ambient ion distributions was found (Ehn et al., 2010). The transmission estimates from that comparison agreed well with the calibrations made in the laboratory, with molecules and clusters as described by Junninen et al. (2010). The fact that the instruments agreed, suggest that no major fragmentation happens inside the APi-TOF.

2.2 Ancillary instrumentation and data analysis

2.2.1 Gas phase sulfuric acid and malonic acid

A chemical ionization mass spectrometer (CIMS, Eisele and Tanner, 1993; Petäjä et al., 2009) measured next to the APi-TOF, providing neutral sulfuric acid concentrations for the measurement period. The CIMS introduces NO_3^- ions into its sample flow, and based on the selectivity of the nitrate ion, only a few stronger acids will transfer a proton to it, the strongest being H_2SO_4. Besides the normal measurement mode of the CIMS, for this period it was also measuring m/Q 103 Th, believed to be de-protonated malonic acid.

2.2.2 Air ion physical characterization

A balanced scanning mobility analyzer (BSMA, Tammet, 2006) also measured during the EUCAARI intensive campaign in Hyytiälä. The BSMA consists of two plane-type differential mobility analyzers, one for each polarity. It scans 16 mobility channels in the range 3.2–0.032 cm^2 V^{-1} s^{-1} with a time resolution of 10 min. The extremely high flow rate of about 3000 l min^{-1} provides good sensitivity and low diffusion losses inside the instrument.

2.2.3 Data analysis

The mass spectra were analyzed using the tofTools toolbox developed by Junninen et al. (2010). The BSMA was used as a reference to account for inlet and transmission losses in the APi-TOF. We compared the total ion concentrations measured by the APi-TOF and the BSMA, and selected appropriate multipliers for the APi-TOF data. The resulting values for the negative ions was 3000, and the positive ions 1000, corresponding to total transmissions of 0.033% and 0.1%, respectively. These values are low compared to the laboratory calibrations performed by Junninen et al. (2010), but the calibrations did not include any inlet losses, and this is believed to be the reason for the discrepancy. The difference between the polarities is most likely due to different tuning of the voltages in the APi.

3 Results and discussion

3.1 Typical features in the mass spectra

3.1.1 Negative spectra

Typical negative ion mass spectra from 80 to 700 Th are presented in Fig. 1, averaged to integer mass resolution for clarity. The spectrum in panel A shows a 3 h average from 09:00–12:00 on 30 April, which was a sunny day and consequently had a high photochemical activity. The ions were dominated by de-protonated sulfuric acid (bisulfate ion HSO_4^-) and its clusters with sulfuric acid and other species.
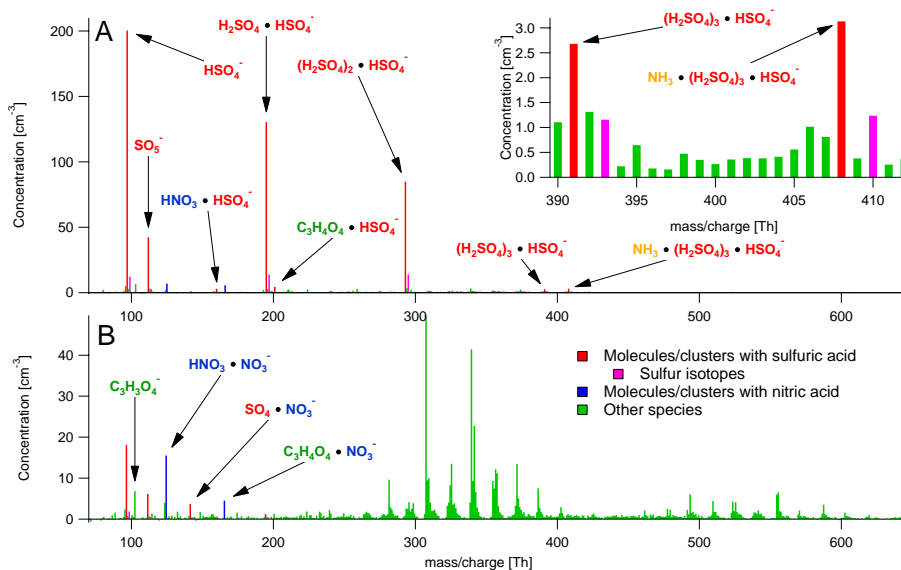
Fig. 1. Negative ion mass spectra during the measurements in Hyytiälä, averaged over 3 h. **(A)** shows a typical daytime spectrum and **(B)** a typical nighttime spectrum. The ions are colored based on the identified composition.

The highest peaks were sulfuric acid monomer (96.96 Th), dimer (194.93 Th) and trimer (292.89 Th). The dimer/trimer in this context refers to a cluster of one/two H_2SO_4 molecules clustered with HSO_4^-. Other selected sulfuric acid peaks are also shown in Fig. 1, including clusters with nitric acid, malonic acid, and ammonia. Additionally, SO_5^- (111.95 Th) was typically detected together with HSO_4^-, and the concentration of SO_5^- was roughly 20% of that of HSO_4^-. Several studies have presented data on HSO_4^- in the atmosphere (e.g. Eisele, 1989b; Eisele et al., 2006), but to our knowledge the only previous atmospheric observations of the SO_5^- ion was by Junninen et al. (2010). Model studies on the role of HSO_5 in the nucleation process has also been performed by Kurtén et al. (2009), and this metastable radical has been found to be significantly stabilized by hydration, i.e. by forming clusters with water molecules, in ambient conditions. However, if SO_5^- would be produced by de-protonation of HSO_5, there would need to be a very high concentration of HSO_5 in the atmosphere, but to our knowledge there are no reports of this. On the other hand, Salcedo et al. (2004) showed that SO_2 can be ionized by CO_3^-, producing end products such as CO_2, SO_3^- an SO_5^-. However, SO_5^- tracks HSO_4^- so closely in our data, that it cannot be formed purely from SO_2 which usually peaks in the early morning.

The range around 400 Th in Fig. 1a is plotted in more detail in the inset figure. During this day we also observed the sulfuric acid tetramer, and the tetramer cluster with ammonia (NH_3). Both of these peaks were very small, but had clear negative mass defects, i.e. the peaks were clearly below the integer masses, distinguishing them from all the surrounding (most likely organic) peaks. The same peaks were observed in the laboratory by Junninen et al. (2010) when mix-

ing a sulfuric acid laden sample with laboratory air. Furthermore, Junninen et al. (2010) did not observe any NH_3 affiliated clusters smaller than the sulfuric acid tetramer, but at the higher masses the NH_3-containing clusters dominated. That may also be the case in this study, but the concentrations of the larger clusters were not high enough to be distinguished. The period shown in Fig. 1 coincided with a strong new particle formation event, as will be shown in Sect. 3.3, and the implications of the observation of a H_2SO_4/NH_3 ion cluster for the nucleation mechanisms are discussed in Sect. 3.4.

Figure 1b shows a 3 h average from 00:00–03:00 on 1 May. During night the H_2SO_4 production was considerably lower, but nevertheless HSO_4^- was still one of the largest peaks in the spectrum. Other distinct peaks were found at 103.00 Th (malonic acid, $C_3H_3O_4^-$), 166.00 Th ($HNO_3 \cdot C_3H_3O_4^-$), 124.98 Th ($HNO_3 \cdot NO_3^-$), and 157.94 ($SO_4 \cdot NO_3^-$). All these have been previously identified by Eisele and Tanner (1990) in Georgia, USA. The last ion may have a different molecular structure but the elemental composition is probably correct.

Based only on the bulk liquid acidity of malonic acid (pKa = 2.83), it is surprising that the ambient concentrations of the ion were so high. However, the gas-phase acidity of small dicarboxylic acids, and especially malonic acid, is considerably higher than what would be expected based on their bulk liquid acidities, as measured by Kumar et al. (2005). They speculated that this is due to the formation of a strong internal hydrogen bond in the corresponding conjugate ions. For instance, for malonic acid, it has been computationally demonstrated (albeit at a fairly qualitative level of theory) that $C_3H_3O_4^-$ prefers a cyclic structure in the gas phase, but an open structure in the aqueous phase (Mavri and Hadzi, 1998).

Our calculations confirm this hypothesis. The minimum-energy structures of de-protonated oxalic, malonic, and succinic acids all contain an internal hydrogen bond (between the remaining COOH hydrogen and the negatively charged oxygen on the COO^- group), as shown in Fig. A1 in Appendix A. However, only the ring in the malonic acid ion contains precisely six atoms, which makes malonic acid a stronger acid in the gas phase than oxalic or succinic acid (calculated proton affinities found in Table A1, Appendix A). More importantly, in the gas phase, malonic acid is also significantly stronger than nitric acid, which explains the abundance of $C_3H_3O_4^-$ measured by the APi-TOF, and why malonic acid can be detected with the CIMS instrument.

The night time spectrum was dominated by a large amount of peaks at high masses. The largest pattern is seen in the range 300–400 Th, with a second pattern forming at 500–600 Th. These peaks have not yet been identified with as high certainty as the previously mentioned ions, partly due to a decrease in the absolute mass accuracy at higher masses, and an increase in the amount of elemental composition permutations possible. A peculiarity is that all the largest peaks between 280 and 400 Th fall on even integer masses. This implies an odd number of N atoms in each ion, according to the nitrogen rule as described in the peak identification section in Junninen et al. (2010).

The instrument transmission for the negative ions during this experiment was optimized for larger masses, and thus there was a sharp cut-off in the lower end of the spectrum. The smallest detectable ions were seen at integer mass 80 Th. This means that we could not detect ions like NO_3^- and CO_3^-. Especially the former is expected to be found in fairly high concentrations based on previous measurements by e.g. Eisele and Tanner (1990) and Junninen et al. (2010).

3.1.2 Positive spectra

The positive ion spectra were more evenly spread out over many masses than the corresponding negative spectra, as seen in Fig. 2. Some positive ion peaks do stick out, mainly n-alkyl pyridines and quinolines, with protonated pyridine at 80.05 Th, and protonated quinoline at 130.07 Th. However, throughout the measurement range there are peaks visible at nearly every mass. The limit at which m/Q we no longer can identify peaks with a high degree of certainty is lower for the positive ions, as the signals are spread out over more masses, yielding generally lower signals. The inset figure shows the mass spectrum in 200–500 Th range, where a pattern typical for organic compounds. Only a daytime spectrum is shown for the positive ions, as the day and nighttime differences are much more subtle than for the negative ions. During the night, the pyridine peaks typically increase around a factor of two, whereas signals at the higher masses decrease.

Similar to the negative ion spectra, also the positive spectra suffer from a sharp transmission cut-off at low masses. The most important ion that we cannot measure is protonated
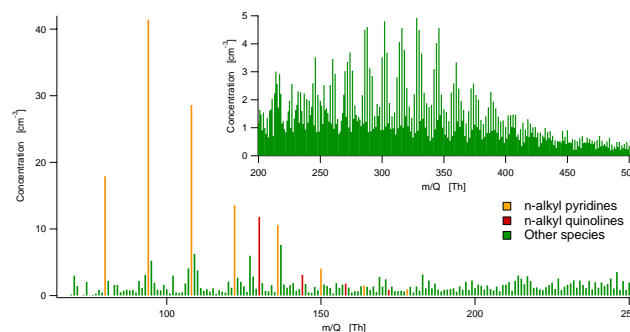
Fig. 2. Typical daytime positive ion mass spectrum during the measurements in Hyytiälä, averaged over 3 h.

ammonia (NH_4^+). If present, also protonated water (H_3O^+) and small protonated water clusters would not have been detected.

3.2 Peak identification

Identifying the elemental composition of the detected peaks was done principally by looking at the high resolution masses. For a mass accuracy of ∼20 ppm in the APi-TOF, the absolute mass can typically be calibrated to up to three decimals, up to a few hundred Thomson. To confirm this first result, and also to provide hints on the chemical formula of the ions, we used time series correlograms and Kendrick analysis (Junninen et al., 2010; Kendrick, 1963). Examples of both these techniques are presented below. A detailed list of all ions identified in this study can be found in the supplementary material, Tables S1 and S2. Tables S3 and S4 list all ions that were detected, but not necessarily identified. The large majority of the identified ions have received their charge by proton transfer to (positive ions) or from (negative ions) the originally neutral molecules. We will refer to protonated and de-protonated ions with the name of the corresponding neutral molecules, except where it may cause confusion.

3.2.1 Negative ions

The time series correlation of each integer mass with other integer masses was calculated after averaging the data to a time resolution of 30 min. Although higher mass resolution data were available, most unit masses were dominated by only one ion, so to optimize the signal to noise for the time series, only unit masses were used for this analysis. Once a correlation was observed, identification was performed based on the high resolution peaks.

Figure 3 shows the time series correlation of each integer m/Q with m/Q 97. These plots, termed (time series) correlograms in this work, were found to be very useful in comparing the temporal behavior of different ions. The peak at m/Q 97 was believed to be dominated by sulfuric
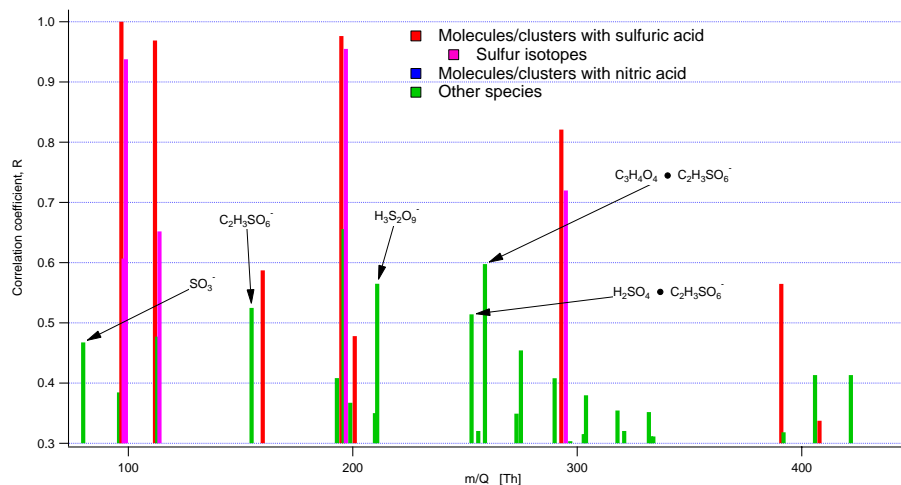
Fig. 3. Correlogram showing time-series correlation of ions with HSO_4^-. The dimer, trimer and tetramer all stand out, together with some other peaks tagged in Fig. 1. Ions with typically lower concentration but high correlation are marked in the figure. The $C_2H_3SO_6^-$ ion may be the first observation of an organosulfate in the gas phase. For reference, the coloring is kept the same as in Fig. 1 although additional peaks were found to contain sulfuric acid.

acid monomer, HSO_4^-, and very high correlations ($R > 0.8$) are found between the monomer and the dimer, trimer and SO_5^-, at masses 195, 293 and 112 Th, respectively. Also the tetramer at 391 Th, and the $HNO_3 \cdot HSO_4^-$ cluster at 160 Th have $R > 0.5$. All of the aforementioned ions were tagged in Fig. 1, and are not tagged in Fig. 3. The peaks tagged in Fig. 3 are those with lower concentrations but that stand out in the correlogram. The first is SO_3^- (at 80 Th), which may correspond to de-protonated HSO_3 which is a short-lived intermediate in the oxidation process of SO_2 into H_2SO_4. Another possibility was mentioned in Sect. 3.1.1, in which SO_3^- is formed directly from reactions between SO_2 and CO_3^- (and possibly other ions). At 211 Th, the peak was identified as having the elemental formula $H_3S_2O_9^-$. This could possibly be an ion cluster of H_2SO_4 and Caro's acid (H_2SO_5), but since the HSO_5^- ion was not separately detected, we could not verify this using correlograms.

At integer m/Q 155 Th, we detected an ion matching the elemental formula $C_2H_3SO_6^-$, and at m/Q 253 and 259 Th its probable clusters with sulfuric and malonic acid, respectively). At unit mass 201 in Fig. 1, the ion $C_4H_5SO_8^-$ was attributed to a cluster of sulfuric and malonic acid ($C_3H_4O_4 \cdot HSO_4^-$). For $C_2H_3SO_6^-$ it is tempting to again assume a cluster with sulfuric acid, which would result in $C_2H_2O_2 \cdot HSO_4^-$, i.e. a cluster of glyoxal and sulfuric acid. The quantum chemical calculations of formation energies of clusters for selected molecules with HSO_4^- (Table A2 in Appendix A) showed that, while malonic acid is strongly bound to HSO_4^-, glyoxal does not bind particularly strongly to it, as could be expected from its low dipole moment and lack of efficiently hydrogen-binding functional groups. In particular, the binding of glyoxal to HSO_4^- is only slightly stronger than that of water to HSO_4^-. Given the much lower concentra-

tion of glyoxal compared to water in the atmosphere, and the fact that the $H_2O \cdot HSO_4^-$ clusters either are not present in the ambient ion distribution, or evaporate in the instrument before they can be detected, it does not seem plausible that the $C_2H_4SO_6^-$ peak would consist of HSO_4^- – glyoxal clusters. We are then left with two alternatives, the peak may correspond to a cluster of some other organic molecule with some other sulfur-containing molecule, or it may correspond to a single molecule. The former was ruled out, as no molecular combinations were found that produced particularly strongly bound clusters. However, the latter possibility is intriguing, as a peak at unit mass 155 Th was observed in the particle phase by Galloway et al. (2009) after reactions of glyoxal oxidation products on ammonium sulfate particles. Based on chromatography experiments, they attributed the peak to glycolic acid sulfate ($C_2H_3O_2HSO_4$).

We computed the proton affinities of both the organosulfate ions proposed by Galloway et al. (2009) (see Fig. A3 in Appendix A for their structures and for more discussion) and we found them to be extremely low; 294.9 and 292.8 kcal mol^{-1} for glyoxal sulfate and glycolic acid sulfate, respectively. These proton affinities are even lower than for HSO_4^-, indicating that these organosulfate ions, if they exist in the gas phase, are likely to be the most stable anions around, and the corresponding neutral organosulfates could be charged even by HSO_4^-. To our knowledge, this would be the first time organosulfates have been identified in the gas phase.

We have also detected another compound, $C_5H_5O_6^-$ (161.01 Th), which can be produced by adding up the elements in malonic acid and glyoxal. However, with the same arguments as above, this is also believed to be a single molecule, possibly a tricarboxylic acid. We
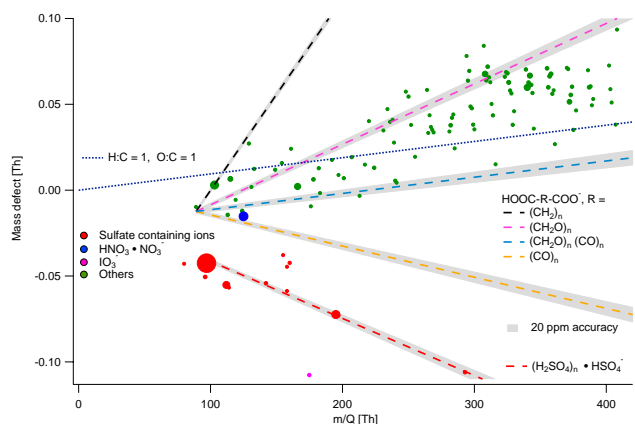
Fig. 4. Mass defects of the negative ion spectrum. The circles are the measured ions, with sizes corresponding to their concentration. Inorganic ions had the lowest mass defects, and the majority of green circles with the highest mass defects are believed to be organic molecules. The dashed lines are examples of where different molecules would show up on the graph. The dotted line corresponds to an organic aerosol ensemble with an O to C ratio of one, and an H to C ratio of one.

earlier speculated that the ion at integer m/Q 259 was $C_3H_4O_4 \cdot C_2H_3SO_6^-$, but it may also be a cluster of $C_5H_6O_6$ with HSO_4^-. The time series correlation between integer m/Q 155 and 259 Th was 0.59, whereas for 161 and 259 Th the corresponding value was 0.52.

The night time negative ion spectrum was dominated by a pattern of peaks at 280–420 Th, with a second similar, but weaker, pattern of peaks at around 460–620 Th. We will here focus on the first pattern, in which the majority of the large ions were found at even integer masses, implying an odd number of N in the molecules. The pattern suggests organic compounds. Based on this assumption, the high resolution masses, and anticipating that each ion contained one N atom, the best guess for the two dominant peaks at integer m/Q 308 and 340 Th, were $C_{10}H_{14}NO_{10}^-$ and $C_{10}H_{14}NO_{12}^-$. Figure S1 in the supplementary material shows how accurately this can be determined for the ion at 340 Th. Two other large peaks at 342 and 372 Th, are proposed to be $C_{10}H_{16}NO_{12}^-$ and $C_{10}H_{14}NO_{14}^-$. The lack of peaks with similar time traces at lower masses suggests that these are single molecules and not clusters. As all of these compounds contain ten carbon atoms, it is tempting to attribute these molecules to highly oxidized products of monoterpenes ($C_{10}H_{16}$). At this high O to C ratio and low H to C ratio, the molecules have to contain a large number of carboxyl groups, which in turn would facilitate that they become ionized and subsequently detected by the APi-TOF. The best correlation at lower masses with the ions at 300–400 Th was found for tartaric ($C_4H_5O_6^-$, 149.01 Th) and malic acid ($C_4H_5O_5^-$, 133.01 Th), which both have very high O to C ratios, possibly produced in reactions leading to fragmentation of the larger ions.

An overview of the entire negative spectrum can be gained by plotting the mass defects, i.e. exact mass – nominal mass, as a function of m/Q (Fig. 4). For instance, the exact mass of HSO_4^- is 96.960 Da, which gives it a mass defect of 96.960 Da–97.000 Da=−0.040 Da. The plotted data are a two-day average, and only peaks with a mean concentration above 0.5 cm^{-3} are plotted for clarity. The size of each marker is a measure of the ion concentration. The inorganic ions are easily distinguished based on their low mass defects. The dashed lines are examples of where specific combinations of functional groups fall on the graph. The shaded area around each line shows the 20 ppm accuracy of the instrument. As all identified organic molecules contain two carboxyl groups (COOH), the origin of these molecular functions is oxalic acid (COOH-COO$^-$). Adding CH_2 groups corresponds to simple dicarboxylic acids (dashed black line), of which malonic acid is the following one. However, for $m/Q > 150$ Th, observed ions clearly have mass defects smaller than the simple dicarboxylic acids, indicative of higher oxygen content. At the other extreme, adding only carbonyl groups (CO, dashed orange line) produces molecules with too low mass defects. The middle two dashed lines (purple and blue) fit the data better, corresponding to additions of only hydroxyl groups (CHOH), or equal amounts of hydroxyl and carbonyl groups, respectively. In reality, the molecules with high carbon number are not expected to be straight chains, in which case they can contain more carboxyl groups, at the same time increasing their charging probability. As seen from the dashed lines, the O to C ratios can be narrowed down fairly well, although the larger organic ions cannot be unambiguously identified. No N atoms were considered here, although the larger molecules were suggested to contain some nitrogen. The mass defect of N itself is only 0.003 and will not shift the molecules very much in Fig. 4. However, adding a functional group containing N may have very different effects, as an amino group (NH_2) has a mass defect of 0.018, and a nitroxy group (NO_3) has a mass defect of −0.012.

Highly oxidized molecules are expected to readily condense onto pre-existing aerosol particles, and the ions present in the negative spectra are assumed to be the most oxidized gas phase molecules. Based on elemental analysis of condensed secondary organics via aerosol mass spectrometry (Aiken et al., 2008), the maximum level of oxidized aerosol corresponds to O:C:H ratio of 1:1:1 (Heald et al., 2010) plotted as the dotted blue line in Fig. 4. Clearly there is overlap of the composition of the observed negative ions with that of condensed SOA, with smaller (<200 Th) and larger (>250 Th) negative ions somewhat more and less oxidized, respectively, than the typical ensemble average for highly oxidized SOA. Moreover, the O:C:H of 1:1:1 corresponds to a carbon oxidation state of +1, consistent with the limiting value discussed by Kroll et al. (2010) for organic oxidation in the atmosphere.

3.2.2 Positive ions

The temporal variability of the positive ions was smaller than that of the negative ions, and thus correlograms were not as effective tools in the peak identification. Mass defect diagrams, as shown in Fig. 4, on the other hand can aid the detection of patterns in the mass spectra when alkyl groups of different lengths are typical building blocks of the ions. This is best done by changing to the Kendrick mass scale (Kendrick, 1963) where the mass of $^{12}CH_2$ is defined as 14.0000. In other words, the measured mass of an ion is divided by $m(^{12}CH_2)/14$, and thus $(CH_2)_n$ will always fall exactly on integer masses. As a result of this, the addition of CH_2 groups will not change the mass defect, and molecule groups differing by $(CH_2)_n$ will form a horizontal line. Figure 5 shows a mass defect diagram in Kendrick mass scale of the positive ion mass spectrum, averaged over two days to include as many ions as possible (for a better comparison with Fig. 4, the unscaled mass defects are plotted in Fig. S2 in the supplementary material). As an example, pyridine and alkyl pyridines all fall on the same horizontal line, denoted $Z = -4$ N. The Z value is described in detail elsewhere (Hughey et al., 2001; Junninen et al., 2010), but briefly, the number is a rough measure of how many rings and/or double bonds the molecules contain. The Z value is defined as $h - 2c$, where the letters signify the amount of H and C atoms in the molecule (as in C_cH_h). If the molecules contain other atoms than C and H, these are listed after the numeric value.

All the molecules with the same Z value belong to the same homologous series. The colored dots on the horizontal lines in Fig. 5 mark where possible ions for each series could be found. The black dots show the ions with even integer masses, whereas the grey triangles represent the odd masses. According to the nitrogen rule, the even masses most likely contain an odd number of N atoms, and the odd masses an even number.

The clearest homologous series in Fig. 5 were -4 N and -10 N, corresponding to alkyl pyridines and alkyl quinolines, respectively. The $Z = -5$ N series is in violation of the nitrogen rule, but is still believed to have been correctly identified. This series starts with $C_6H_7N^+$, which is the elemental formula of phenylamine (aniline), but in this case it would have been charged by loss of an electron and not by addition of a proton as is the case for practically all other identified species. Another possibility is that $C_6H_7N^+$ forms a stable seven membered ring of some sort. The $Z = 0$ N and $Z = -2$ N series are classified as alkyl pyrrolines and pyrroles, respectively. The 4N series corresponds to alkyl amines, which may be an important precursor for new particle formation (Loukonen et al., 2010; Smith et al., 2009). A large peak at 214 Th may be an amine ($C_{14}H_{32}N^+$), but this could not be reliably determined. Recently Smith et al. (2009), measured the chemical composition of 10 nm particles during a nucleation event in Hyytiälä, and found that the new particles contained considerable amounts of amines
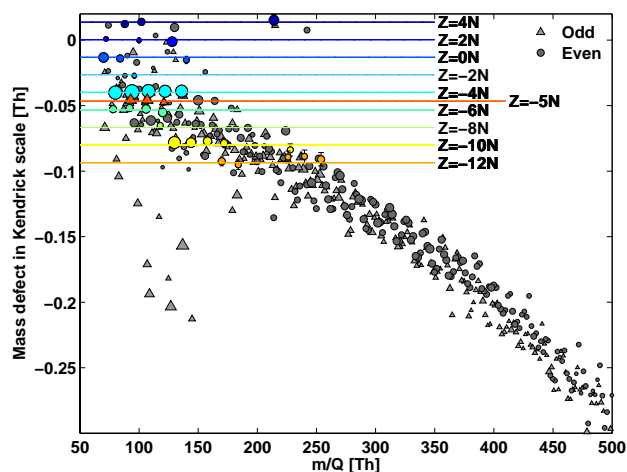

Fig. 5. Mass defects in Kendrick mass scale of the positive ion spectrum. The mass defect becomes lower with increasing mass, possibly due to increasing ring structures, or additions of N and/or O. The clearest homologuous series is that of alkyl pyridines at $Z = -4$ N, and quinoline at $Z = -10$ N.

(23% of the detected ions were attributed to aminium salts). The ion at m/Q 74 Th close to the 4 N line has been identified as an amine, but in the two day average used for this analysis, there is a double peak at this m/Q and thus the exact mass is not fit accurately enough for it to fall on the 4 N line.

One major feature of the positive mass spectrum is a steady decrease in the mass defect in the Kendrick mass scale with increasing m/Q (Fig. 5). Based on the ions identified so far, most of the positive ions include only C and H atoms, together with one N. If this is true also for the larger ions, they will most likely contain more ring structures, as the addition of CH_2 groups would not cause a decrease in the mass defect. Other possibilities are the additions of more nitrogen and oxygen. In Fig. 5, the majority of the ions fall closely on a decreasing curve, but there were approximately 10 ions, all at even masses in the range 70–150 Th, that clearly fell below this curve. Most of these have not been identified yet, but many of them seem to cluster readily with water. For instance, a series of peaks at 108.92, 126.93, and 144.94 Th are all separated by 18.01 Th, the mass of water being 18.010 Da.

Considering the typical compounds identified in the positive and negative ion spectra, an additional important result was that the average bulk densities are very different between the polarities. The highly oxidized negative ions had very few H atoms, and the densities were mostly around $1.6 \, g \, cm^{-3}$ or above, whereas the positive ions contained very few O atoms, and were often composed of several straight chain alkyl groups, with densities around $1.0 \, g \, cm^{-3}$ or below. This difference becomes particularly crucial when comparing the ion mobility measurements of positive and negative ions, where ions with the same mass have different mobilities depending on their density (Ku and de la Mora, 2009; Ehn et al., 2010).
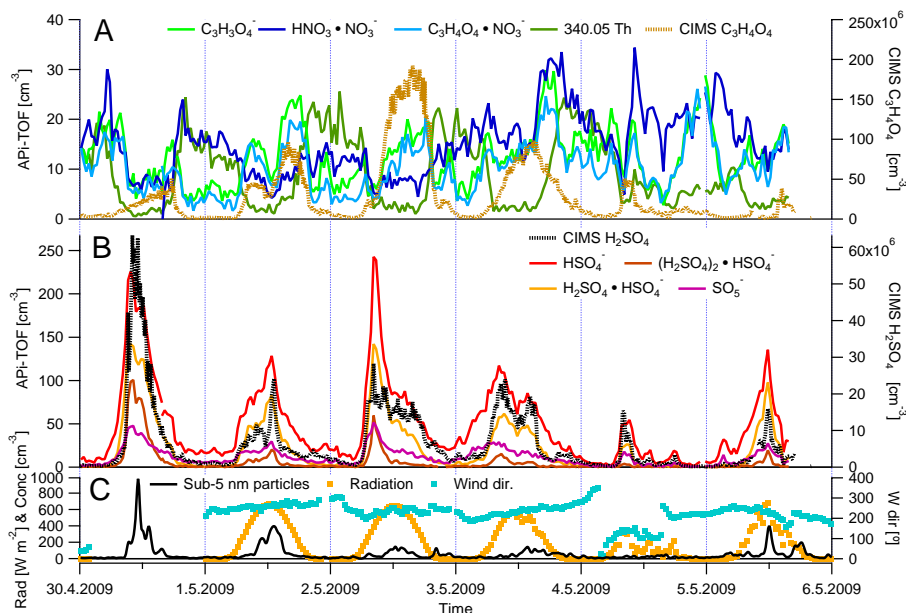
Fig. 6. Time trends of selected negative ions in Hyytiälä measured by the APi-TOF, with sulfate – related ions in the middle panel and nitric acid and organics in the top panel. Also included in these are CIMS measurements of sulfuric and malonic acid (dotted lines). In the bottom panel radiation and wind direction are included (data for 30 April is missing), together with the concentration of sub-5 nm particles.

3.3 Time series and diurnal cycles

Owing to the high sensitivity of the APi-TOF, reasonable mass spectra could typically be observed for 5 min averaging. The longer the average, however, the better the obtained signal-to-noise ratio. When analyzing the time series of the selected ions, we used 30 min averages. Figure 6 shows the temporal behavior of some previously mentioned ions, together with CIMS measurements (dotted lines) of H_2SO_4 and $C_3H_4O_4$, and particle, radiation and wind direction measurements at SMEAR II.

All the sulfuric acid related peaks had very similar time trends (panel B), as expected based on the high correlations presented in Fig. 3. The temporal behavior of HSO_4^- measured by the APi-TOF and neutral H_2SO_4 concentration reported by the CIMS agreed very well. This was not surprising as HSO_4^- is one of the anions with the lowest proton affinity, and is therefore very unlikely to transfer its charge upon collisions with other molecules. Thus the concentration of HSO_4^- should follow the concentration of the neutral H_2SO_4. This is not the case for the ions of weaker acids, which are limited not only by the neutral parent concentration, but also by the concentration of all the stronger acids to which they upon collision will donate their charge.

In Fig. 6a, the ion at 340.05 Th was used as a surrogate for all the night time molecules observed at the high masses, as their time behavior was similar. During the daytime, the signal of these peaks was down by a factor of 10 or more from their nighttime values. The malonic acid (103.00 Th) and malonic/nitric acid cluster (166.00 Th) signals tracked

each other very closely indicating that the cluster concentration was mainly dependent on the malonic acid signal. The CIMS was designed and calibrated to measure sulfuric acid, but in this campaign it was also set to measure malonic acid. The ion signal was converted to a neutral concentration in the same way as for sulfuric acid and with the same calibration coefficient (Petäjä et al., 2009), which could introduce a bias. Nevertheless, during certain periods such as May 1 the trends were very similar. Malonic acid also seemed to be photochemically produced as the highest concentrations were observed during the sunny days.

Finally, the nitric acid dimer (124.98 Th) did not seem to have any clear diurnal cycle, although there was a fair amount of variability. As the H_2SO_4 dimer tracked the monomer very well, we assumed that the nitric acid dimer also gave some representation of the nitric acid monomer behavior although we did not directly measure it due to negligible transmission below 80 Th for the APi-TOF configuration during this study.

For a closer look at average diurnal patterns, we plotted some selected negative ions as a function of time of day (Fig. 7) for the period shown in Fig. 6. Some picture of the prevailing meteorology during this period is seen in Fig. 6c. Pure sulfuric acid peaks and SO_5^- behaved in a very similar way, roughly following the radiation intensity. SO_3^- was at the edge of our transmission curve, and the signal was therefore very low, but it also seemed to track the HSO_4^- signal. On the other hand, when clustered with NO_3^-, both SO_3 and SO_4 peaked in the early morning, as did pure SO_4^-. This may
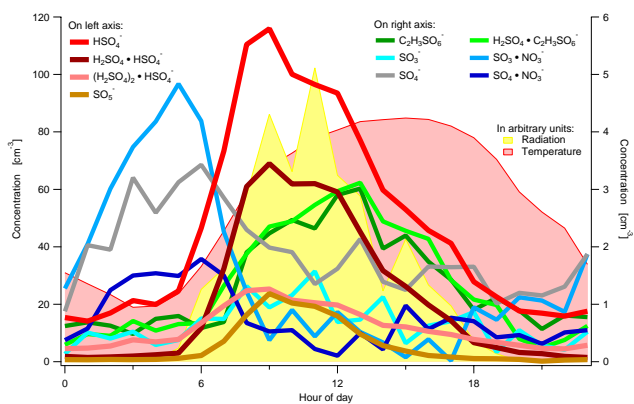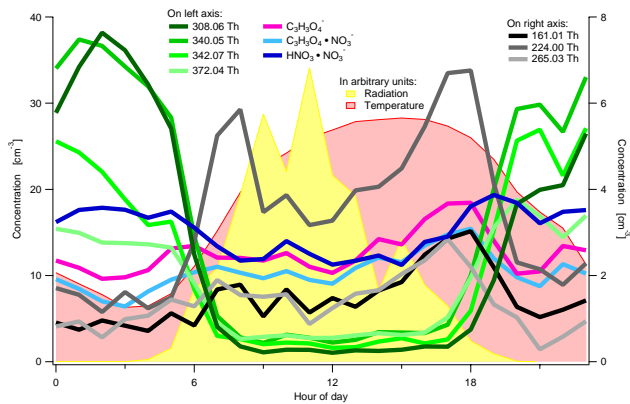
Fig. 7. Diurnal trends for selected sulfuric acid related negative ions. The data is averaged over 30 April–5 May, 2009.

Fig. 8. Diurnal trends for selected organic and nitric acid negative ions. The data is averaged over 30 April–5 May, 2009.

be a result of SO_2 typically peaking in the early morning, and as briefly discussed in Sect. 3.1.1, being ionized to form SO_3^- and possibly other charged sulfur oxides.

The two green traces representing the organosulfate and its cluster with H_2SO_4 peaked in the afternoon, when the H_2SO_4 concentration was already going down. This could have been caused by a higher concentration of glyoxal (or its oxidation products) in the afternoon, producing more organosulfates through gas phase reactions at that time. Another possibility is that, as these molecules have been found in aerosol particles (Galloway et al., 2009), the formation occurred via heterogeneous reactions inside the particles and a small amount evaporated and was subsequently detected in the gas phase. This would explain the diurnal behavior which peaked a few hours after H_2SO_4, and thus a large amount of H_2SO_4 had already condensed onto the particles, increasing the probability of reactions in the particle phase. Although evaporation of an organosulfate is thought to be very unlikely, the concentration peaked at the same time as the ambient temperature reached its maximum value, making it the most probable period when evaporated species could be detected. In Fig. 2 by Eisele et al. (2006), they presented a mass spectrum of negative ions measured during high H_2SO_4 concentrations. It showed a large unidentified peak at integer m/Q 253 Th, and possibly a smaller peak at 155 Th, perhaps corresponding to a cluster of the organosulfate with sulfuric acid, and the pure organosulfate, respectively, suggesting that these are not specific to Hyytiälä.

As seen in Fig. 8, malonic acid, nitric acid, and their cluster had very weak diurnal cycles. At the other extreme, the ions around 300–400 Th peaked during the night and were 10–20 times lower during the day. There was also an internal pattern visible, with 372.04 Th peaking first, and 308.06 Th peaking last. Assuming that the peaks were correctly identified as $C_{10}H_{14}NO_{14}^-$ and $C_{10}H_{14}NO_{10}^-$, this implies that the relative abundance of the most oxidized ions like 372.04 (O:C = 1.4) decreased during the night, and less oxidized

ions like 308 (still with O:C = 1) increased. This makes sense qualitatively, as the primary night time oxidation happens by O_3 and NO_3 (which is formed from O_3), and the O_3 in Hyytiälä usually decreased during night to reach a minimum in the early morning.

The last three plotted ions in Fig. 8 are related to the 161.01 Th peak ($C_5H_5O_6^-$, possibly a tricarboxylic acid). In addition to $C_5H_5O_6^-$, its clusters with nitric acid and with malonic acid were detected at m/Q 224.00 and 265.03 Th, respectively. The diurnal patterns of these peak in the evening, with a local maximum in the early morning. In the previously discussed Fig. 2 in Eisele et al. (2006), a peak at 224 Th is tagged, possibly corresponding to $HNO_3 \cdot C_5H_5O_6^-$.

The time traces for positive ions (Fig. 9) do not show as much variability as the negative ions. All the n-alkyl pyridines, which are the most abundant ions, correlate fairly well with the exception of pure (protonated) pyridine, which at times even seems to anti-correlate with the pyridines with alkyl groups. The quinolines track both each other and most of the pyridines, implying that either the sources for these are the same, or that the lifetime of these molecules in the atmosphere is long enough that the ion concentration variations are controlled by the total amount of ions available.

Some ions that show more temporal variability are plotted in the bottom panel of Fig. 9. A very interesting ion was the tropylium ion $C_7H_7^+$ (91.05 Th), to our knowledge measured for the first time in ambient air, which is the only positive ion that we have identified which did not contain a nitrogen atom. The largest amine peak was $C_6H_{16}N^+$ detected at 102.13 Th, possibly corresponding to triethyl amine. Some sharp peaks of short duration in time suggest that they may have a local source nearby, as these peaks are not seen in the other traces and is thus not due to total ion fluctuations. Finally, ion 302.2 Th, representing the organic pattern between 250 and 400 Th, showed the clearest diurnal pattern, peaking in the early afternoon and thus anti-correlating with the pattern of ions at the same masses in the negative spectrum.
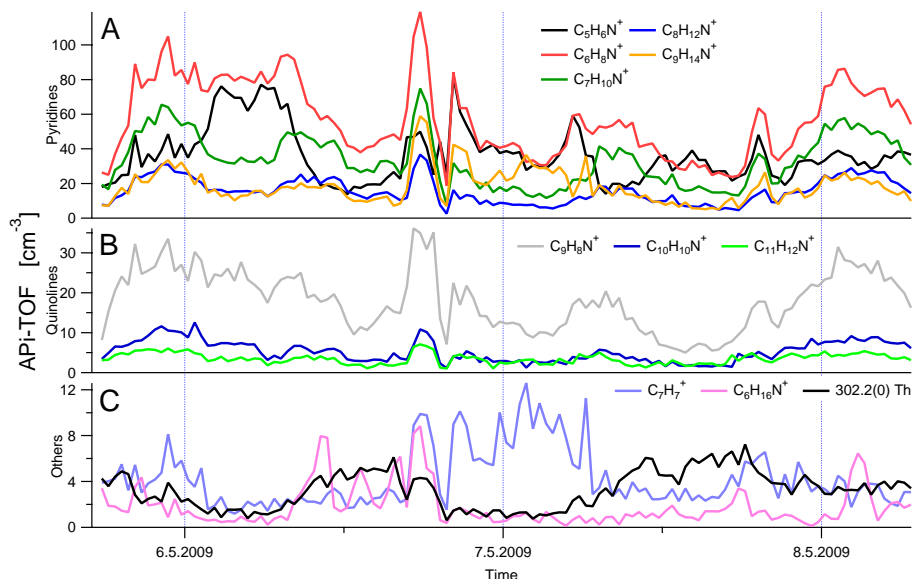
Fig. 9. Time trends of selected positive ions in Hyytiälä measured by the APi-TOF, with pyridines in the top panel, quinolines in the middle, and other ions in the bottom panel.

3.4 Implications for new particle formation mechanisms

Ion-induced nucleation typically accounts for about 10% of the total nucleation in Hyytiälä (Gagné et al., 2009, and references therein). If the majority of the nucleation and growth occurs via neutral pathways, we must assess what insight into the new particle formation we can gain through the investigation of ambient ions.

The main candidate for the initial nucleation steps has long been sulfuric acid (Weber et al., 1997; Kulmala et al., 2006). Since sulfuric acid ionizes very easily, the APi-TOF is very sensitive to it, and also its clusters, as shown above. The composition of the neutral clusters and molecules and the ions are not expected to be exactly the same, but the ion composition is governed by available neutral molecules. The total ion concentration is determined by production (mainly cosmic rays/radon) and loss (coagulation/deposition/recombination) rates, but the distribution of the ions is determined by the concentrations and proton affinities of the neutral molecules/clusters. If the composition of the new particles/clusters is mainly sulfuric acid, then they should also be easily ionized and thus detected by the APi-TOF. At ambient pressure and RH, most neutral sulfuric acid molecules and clusters will have water molecules attached to them. Although to a much lesser extent than ammonia or amines, water can also stabilize pure sulfuric acid clusters. Recently Smith et al., 2009, proposed that the stability of newly nucleated particles is largely due to acids and bases forming salts. In this case, the APi-TOF would be optimal for measuring the precursor vapors, as the strongest bases and acids should make the most stable salts, and should also

be most easily ionized in the atmosphere. However, once the salts have been formed in the new particles/clusters, they will no longer become easily charged, and any mass spectrometric detection with the APi-TOF without a charging mechanism is no longer possible.

Although only clearly visible during one day, the detection of the sulfuric acid tetramer clustered with ammonia can be a very strong indication of a particle formation pathway. As seen in Fig. 6c, the highest sub-5 nm concentrations were also measured during that specific day. According to the results of Hanson and Lovejoy (2006) and Ortega et al. (2008) pure, neutral sulfuric acid clusters are not thermodynamically stable enough to be present in any significant concentrations in the lower troposphere. However, if negatively charged, or if clustered with e.g. ammonia or amines, the clusters become much more stable. The observation of clusters with the APi-TOF requires them to be charged, but the evaporation rate of NH_3 from ion clusters with low H_2SO_4/NH_3 ratio is very high (Hanson and Lovejoy, 2006), which explains why we have not measured ammonia clustered with the H_2SO_4 dimer or trimer. The detection of a charged sulfuric acid/ammonia cluster strongly implies the presence of many more of corresponding neutral clusters.

Amines were detected in the positive ion spectrum, and although not the dominant species, the importance of these may be significant in nucleation even at low concentrations as they can stabilize sulfuric acid clusters even more efficiently than ammonia (Loukonen et al., 2010). No sulfuric acid/amine clusters were observed in our measurements, indicating that the concentration of ammonia was higher than any of the amines, as could be expected. However, as typical particle formation rates during new particle formation

in Hyytiälä is of the order of $1\,cm^{-3}\,s^{-1}$ (Manninen et al., 2009a; Dal Maso et al., 2005), the absolute cluster concentrations need not be very high to be important.

Organosulfates were identified in the gas phase, implying that chemical reactions of sulfuric acid in the gas or particle phase are occurring during photochemical production of H_2SO_4 and secondary organics. The importance of this finding is still unclear. The same organosulfate was detected previously in a chamber study (Galloway et al., 2009), and possibly also observed (though not firmly identified) on another continent (Eisele et al., 2006).

4 Conclusions

The APi-TOF was deployed in a boreal forest site in southern Finland, where it measured the composition of positive and negative ambient ions. Although the reported measurements only cover 9 days during the peak new particle formation season in Hyytiälä, we believe that these measurements make a good representation of spring/early summer time ion composition and dynamics in this region. The elemental composition of close to 80 ions was identified with a high degree of certainty. Several of these ions were identified for the first time, and for many ions also the molecular formulas were estimated. Quantum chemical calculations were carried out to assist the identification process. A list of all identified ions is given in the supplementary material, together with a complete list of masses of all observed ions.

During sunny days the negative ion spectrum is dominated by sulfuric acid and its clusters. SO_5^- was also observed, usually making up $\sim$20% of the HSO_4^- signal. The di-, tri-, and tetramer sulfuric acid clusters correlated with new particle formation events in Hyytiälä, in line with studies on the important role of sulfuric acid in atmospheric nucleation (Weber et al., 1997; Petäjä et al., 2009; Sipilä et al., 2010). Additionally, the sulfuric acid tetramer was found in a cluster with ammonia, suggesting that sulfuric acid/ammonia nucleation may be significant in Hyytiälä. The observation of a H_2SO_4/NH_3 ion cluster means that these clusters are abundant in the neutral cluster distributions.

No strong diurnal behavior was seen in the positive ion spectrum. In both day and night time, the spectrum below 200 Th was dominated by alkyl pyridines and quinolines, and at 200–400 Th a more continuous spectrum of peaks was visible. Kendrick analysis revealed additional homologous series below 200 Th, of alkyl amines, pyrroles, and pyrrolines.

The first observations of organosulfates in the gas phase were made during this study, possibly formed from the reaction of sulfuric acid with the oxidation products of glyoxal, either in the particle phase or the gas phase. Whatever the formation mechanism, these organosulfates are expected to be extremely low-volatile, and formed from sulfuric acid, a low-volatility trace gas itself, making the expected concentrations extremely low. Nevertheless, they are visible in the

ion spectrum, proving how sensitive the APi-TOF can be to certain species. The importance of these molecules for new particle formation is still unclear.

During night, the negative ion spectrum was dominated by ions in the range 280–420 Th. These are thought to be highly oxygenated organic acids, possibly formed from the oxidation of monoterpenes emitted from the vegetation, but more work needs to be done to confirm the composition of these ions, as is the case with the ions at similar masses in the positive spectrum. The average mass defect of the negative ions corresponds to O:C:H ratio of 1:1:1, very similar to the composition of highly oxidized organics observed in secondary aerosol via high resolution mass spectrometry.

We established the APi-TOF measurements of ambient ions as a powerful tool in studying nucleation in the atmosphere, whether neutral or ion-induced. In the future, the peak identification schemes will be improved and the APi-TOF instrument as an ambient ion detector will be deployed in various environments to probe the differences in the chemical composition of the atmospheric ions. Ionization schemes will be developed to be able to quantitatively investigate the composition of neutral clusters in the atmosphere.

Appendix A

Quantum chemical calculations

A1 Computational details

All calculations were performed using the Gaussian 09 program suite (Frisch et al., 2009) and the CBS-QB3 method (Montgomery et al., 1999, 2000). CBS-QB3 is a composite method involving geometry optimizations and harmonic vibrational frequency calculations with the B3LYP density functional and a triple-zeta basis set, followed by a series of energy calculations aiming at estimating the basis-set limit CCSD(T) energy. Errors in vibrational frequencies and the imbalance of electron spin contributions are accounted for by using empirical scaling factors. For a test set of single molecules, the CBS-QB3 binding energies are accurate to within about 1 kcal/mol (Montgomery et al., 2000). Proton affinities (PA) for all species X were computed as -1 times the standard (298 K and 1 atm reference pressure) enthalpy change of the $X+H^+ => XH^+$ reaction, with the enthalpy of the free proton taken to be exactly $2.5\,RT$, where R is the gas constant. Gas-phase acidities (GA) for all species XH were similarly computed as the standard (298 K and 1 atm reference pressure) Gibbs free energy change of the $XH => X^- + H^+$ reaction, with the entropy of the free proton computed from the translational partition function as 26.013 cal/K mol at 298.15 K. It should be noted that somewhat counter-intuitively, low numerical values for proton affinities or gas-phase acidities correspond to strong acids. In the text, "high gas phase acidity" will refer to strong acidity
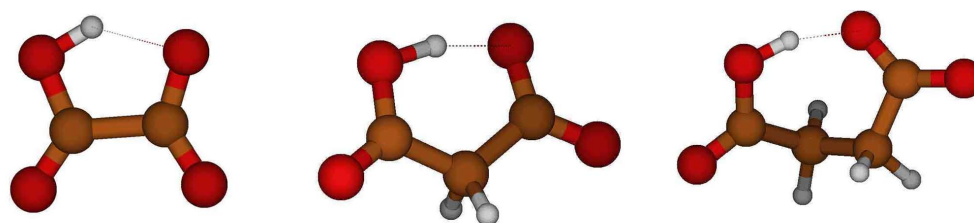
Table A1. Deprotonation electronic energies, conjugate anion proton affinities and gas-phase acidities for selected acids, computed at the CBS-QB3 level.

Species	Deprotonation ΔE_{elec}, kcal/mol	Proton affinity of conjugate anion, kcal/mol	Gas-phase acidity, kcal/mol
$C_2H_2O_4$ (oxalic acid)	329.6	322.6	314.6 (316.2 $\pm$ 0.15[a])
$C_3H_4O_4$ (malonic acid)	326.5	318.2	311.3 (314.8 $\pm$ 0.03[a])
$C_4H_6O_4$ (succinic acid)	331.1	322.8	316.3 (317.8 $\pm$ 0.01[a])
HNO_3 (nitric acid)	332.1	323.5 (324.5 $\pm$ 0.2[b])	317.2 (317.8 $\pm$ 0.2[b])
CH_3SO_3H (methylsulfonic acid)	323.5	317.3	310.5 (315.0[a])
H_2SO_4 (sulfuric acid)	317.4	311.1 (306.4 $\pm$ 3.1[c])	302.7 (299.0 $\pm$ 3.1[c])

[a] Experimental value, (Kumar et al., 2005);

[b] Experimental value; (Davidson et al., 1977);

[c] Experimental value, (Wang et al., 2000).

Fig. A1. Minimum-energy structures (at the CBS-QB3 level) of hydrogenoxalate (left), hydrogenmalonate (center) and hydrogensuccinate (right) ions. Color coding: red = oxygen, brown = carbon, white = hydrogen.

in the chemical sense (i.e. low numerical PA values for the conjugate ions or low numerical GA values for the acids).

## A2 Computed proton affinities and gas-phase acidities, and error analysis

The computed de-protonation electronic energies (not including zero-point energies), conjugate base anion proton affinities and gas-phase acidities for oxalic, malonic, succinic, nitric, sulfuric and methylsulfonic acid are given in Table A1. Available experimental data are also given. All data agree on the general relative ordering of these six species. In the gas phase, sulfuric acid is the strongest acid, followed by methylsulfonic, malonic, oxalic, succinic and nitric acid. The values for methylsulfonic and malonic acid are very close to each other, as are the values for succinic and nitric acid.

As shown in Fig. A1, the hydrogenoxalate, hydrogenmalonate and hydrogensuccinate ions all contain an internal hydrogen bond. While the rings formed by the hydrogen bonding in the hydrogenoxalate and hydrogensuccinate ions contain five and seven atoms, respectively, and are somewhat strained, the ring in the hydrogenmalonate ion contains precisely six atoms, and is hence much stronger. This is reflected in the computed hydrogen bond lengths (1.669 Å for hydrogenoxalate, 1.364 Å for hydrogenmalonate and 1.437 Å for hydrogensuccinate) as well as the proton affinities of the ions and gas-phase acidities of the acids (Table A1).

Given the 1 kcal/mol accuracy of the CBS-QB3 method for the test set of Montgomery et al., 2000, the differences of around 2–4 kcal/mol between the experimental and computed proton affinities or gas-phase acidities for all but the nitric and succinic acids (and corresponding ions) are both surprising and disappointing. For oxalic and malonic acid, part of the difference between computed and measured values is likely caused by internal rotations in the neutral acid molecules, which serve to lower the entropy and thus stabilize the neutral acids compared to the more rigidly bound ions. This leads to larger GA values (weaker acidities) than predicted using the harmonic oscillator approximation. Test calculations using the hindered rotor package of the Gaussian 09 program indicate that the magnitude of this error is around 0.5 kcal/mol with respect to the free energies. The free acids are also likely to have a larger number of low-energy conformers, which might further increase their entropy, and affect the GA values by a similar amount. For sulfuric acid, part of the errors in the free energies are likely caused by the internal rotations of the HSO_4^- ion, as described e.g. by Kurtén et al. (2007). Methylsulfonic acid may be associated with similar problems due to the almost unhindered rotation of the methyl group.

An even larger problem than the internal rotations is the inaccurate description of the vibrations of the functional groups involved in the strong internal hydrogen bond of the hydrogenmalonate ion. This hydrogen bond is extremely short,
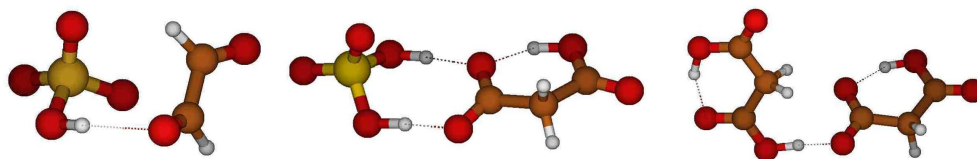
Fig. A2. Minimum-energy structures of the $HSO_4^- \cdot C_2H_2O_2$ (left) $HSO_4^- \cdot C_3H_4O_4$ (middle) and $C_3H_3O_4^- \cdot C_3H_4O_4$ (right) clusters, at the CBS-QB3 level. Color coding: yellow = sulfur, red = oxygen, brown = carbon, white=hydrogen. Note that the minimum-energy structure of $HSO_4^- \cdot C_3H_4O_4$ actually corresponds to $H_2SO_4 \cdot C_3H_3O_4^-$ as the negatively charged carbonyl oxygen is stabilized by two strong hydrogen bonds (one intramolecular and the other intermolecular). Also, the $C_3H_3O_4^- \cdot C_3H_4O_4$ minimum-energy structure is predicted to contain only one intermolecular hydrogen bond, as two of the hydroxyl groups prefer to participate in intramolecular bonds.
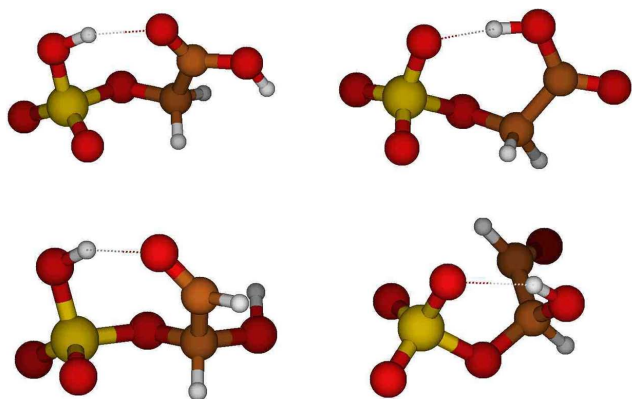
Fig. A3. Minimum-energy structures of the neutral (left) and ionic (right) forms of glycolic acid sulfate (top) and glyoxal sulfate (bottom), at the CBS-QB3 level. Color coding: yellow = sulfur, red = oxygen, brown = carbon, white = hydrogen.

Table A2. CBS-QB3 formation enthalpies and free energies (at 298 K and 1 atm reference pressure) for selected anion dimer clusters.

Species	Formation $\Delta H°$, kcal/mol	Formation $\Delta G°$, kcal/mol
$HSO_4^- \cdot C_2H_2O_2$	−18.2	−6.6
$HSO_4^- \cdot C_3H_4O_4$	−36.7	−23.6
$C_3H_3O_4^- \cdot C_3H_4O_4$	−32.2	−21.3
$HSO_4^- \cdot H_2O$	−13.5	−5.1
$HSO_4^- \cdot H_2SO_4$	−49.2	−35.7

and the potential energy surface is described by a double well rather than a single minimum. This leads to very large errors in the computed vibrational frequencies. Instead of one typical bonded O-H stretching vibration around $3000\,cm^{-1}$, the hydrogenmalonate ion has four different vibrations in the region between 1500 and $2000\,cm^{-1}$, all of which correspond to some type of motion of the O-H...O group. A test calculation at the MP2/6-311++G(2d,2p) level yielded a similar structure and similar frequencies, indicating that the problem is neither the lack of diffuse functions in the basis set nor the (known) deficiencies in the B3LYP description of hydrogen bonding. An anharmonic frequency calculation using the same level of theory as the CBS-QB3 geometry optimization (B3LYP/6-311G(d,p)) decreased two of the O-H...O group's vibrational frequencies to below $800\,cm^{-1}$ (a decrease of over $1000\,cm^{-1}$!) indicating the large effect of the double well potential on the computed values. Note that the anharmonic frequencies, which are also computed assuming a single minimum, are certainly not a good starting point for entropy calculations, either – they simply illustrate the magnitude of the problem. A full statistical-mechanical treatment of vibrational motion in a multidimensional double-well po-

tential is beyond the scope of this study. Similar problems are encountered in treating the short internal hydrogen bond of butene diol (H. Kjaergaard, personal communication, 2010).

Other possible error sources, in addition to inaccuracies in the CBS-QB3 energies, may include different definitions for the thermodynamic values for the free proton, as well as issues related to the choice of reference compounds in the experiments. For our purposes, the precise values in any case matter less than the relative ordering, on which all the different data agree.

A3 Clustering

To investigate the possible chemical identity of the peaks seen at 155 and 201 Th (corresponding to elemental compositions of $C_2H_3SO_6^-$ and $C_4H_5SO_8^-$, respectively) we computed the formation enthalpies and free energies of clusters of HSO_4^- with glyoxal and malonic acid, as these could explain the two peaks. Several structural isomers have been studied for each cluster type, but only the most stable ones are displayed and discussed here. These are given in Table A2. The corresponding cluster structures are shown in Fig. A2. Shown also for comparison are the binding energies for $HSO_4^- \cdot H_2O$ and $HSO_4^- \cdot H_2SO_4$ clusters, as well as the malonic acid – hydrogenmalonate cluster. We also computed the CBS-QB3 proton affinities of both organosulfate ions that could explain the ion at 155 Th (see Fig. A3 for their

structures). As for hydrogenmalonate, the low proton affinities are caused by the formation of very strong intermolecular hydrogen bonds in the ions.

When comparing clusters of HSO_4^- with sulfuric acid and malonic acid, it should be noted that the evaporation rates corresponding to these formation free energies are both low enough to be completely negligible. Evaporation rates are on the order of $10^{-16}\,s^{-1}$ and $10^{-8}\,s^{-1}$ for $HSO_4^- \cdot H_2SO_4$ and $HSO_4^- \cdot C_3H_4O_4$, respectively. Thus, the difference in the formation free energies does not in practice play a role in determining their relative concentrations. For practical purposes, whenever a cluster of HSO_4^- with sulfuric or malonic acid is formed, it never evaporates, but is removed solely by growth, coagulation and/or neutralization. Similar considerations very probably apply also for clusters of the hypothetical 155 Th organosulfate ion with other strong acids such as sulfuric acid. It is important to stress that the concentrations of the small ionic clusters is not in thermodynamic equilibrium (in which e.g. free HSO_4^- would not exist at all) but at best in a dynamic steady state, to which the evaporation in the measurement instrument adds its own signature.

Supplementary material related to this article is available online at: http://www.atmos-chem-phys.net/10/8513/2010/ acp-10-8513-2010-supplement.pdf.

References

Aiken, A. C., DeCarlo P. F., Kroll, J. H., Worsnop, D. R. Huffman, J. A., Docherty, K., Ulbrich, I. M., Mohr, C., Kimmel, J. R. Sueper, D., Zhang, Q., Sun, Y. Trimborn, A., Northway, M., Ziemann, P. J., Canagaratna, M. R., Onasch, T. B., Alfarra, R., Prevot, A. S. H., Dommen, J., Duplissy, J., Metzger, A., Baltensperger, U., and Jimenez J. L.: O/C and OM/OC Ratios of Primary, Secondary, and Ambient Organic Aerosols with High Resolution Time-of-Flight Aerosol Mass Spectrometry, Environ. Sci. Technol., 42, 4478–4485, doi:10.1021/es703009q, 2008.

Andreae, M. O. and Rosenfeld, D.: Aerosol-cloud-precipitation interactions. Part 1. The nature and sources of cloud-active aerosols, Earth-Sci. Rev., 89, 13–41, doi:10.1016/j.earscirev.2008.03.001, 2008.

Asmi, E., Sipilä, M., Manninen, H. E., Vanhanen, J., Lehtipalo, K., Gagné, S., Neitola, K., Mirme, A., Mirme, S., Tamm, E., Uin, J., Komsaare, K., Attoui, M., and Kulmala, M.: Results of the first air ion spectrometer calibration and intercomparison workshop,

Atmos. Chem. Phys., 9, 141–154, doi:10.5194/acp-9-141-2009, 2009.

Dal Maso, M., Kulmala, M., Riipinen, I., Wagner, R., Hussein, T., Aalto, P. P., and Lehtinen, K. E. J.: Formation and growth of fresh atmospheric aerosols: eight years of aerosol size distribution data from SMEAR II, Hyytiälä, Finland, Boreal Env. Res., 10, 323–336, 2005.

Davidson, J. A., Fehsenfeld, F. C., and Howard, C. J.: Heats of Formation of NO_3- and NO_3- Association Complexes with HNO_3 and HBr, Int. J. Chem. Kinet., 9, 17–29, 1977.

DeCarlo, P. F., Kimmel, J. R., Trimborn, A., Northway, M. J., Jayne, J. T., Aiken, A. C., Gonin, M., Fuhrer, K., Horvath, T., Docherty, K. S., Worsnop, D. R., and Jimenez, J. L.: Field-deployable, high-resolution, time-of-flight aerosol mass spectrometer, Anal. Chem., 78, 8281–8289, doi:10.1021/Ac061249n, 2006.

Ehn, M., Junninen, H., Schobesberger, S., Manninen, H. E., Franchin, A., Sipilä, M., Petäjä, T., Kerminen, V.-M., Tammet, H., Mirme, A., Mirme, S., Hõrrak, U., Kulmala, M., and Worsnop, D. R.: An instrumental comparison of mobility and mass measurements of atmospheric small ions, Aerosol Sci. Tech., submitted, 2010.

Eisele, F. L.: Natural and transmission line produced positive ions, J. Geophys. Res. A., 94, 6309–6318, 1989a.

Eisele, F. L.: Natural and anthropogenic negative ions in the troposphere, J. Geophys. Res. A., 94, 2183–2196, 1989b.

Eisele, F. L. and Tanner, D. J.: Identification of ions in continental air, J. Geophys. Res. A., 95, 20539–20550, 1990.

Eisele, F. L. and Tanner, D. J.: Measurement of the gas-phase concentration of H_2SO_4 and methane sulfonic-acid and estimates of H_2SO_4 production and loss in the atmosphere, J. Geophys. Res. A., 98, 9001–9010, 1993.

Eisele, F. L., Lovejoy, E. R., Kosciuch, E., Moore, K. F., Mauldin, R. L., Smith, J. N., McMurry, P. H., and Iida, K.: Negative atmospheric ions and their potential role in ion-induced nucleation J. Geophys. Res. A., 111, D04305, doi:10.1029/2005jd006568, 2006.

Enghoff, M. B. and Svensmark, H.: The role of atmospheric ions in aerosol nucleation – a review, Atmos. Chem. Phys., 8, 4911–4923, doi:10.5194/acp-8-4911-2008, 2008.

Frisch, M. J., Trucks, G. W., Schlegel, H. B., Scuseria, G. E., Robb, M. A., Cheeseman, J. R., Scalmani, G., Barone, V., Mennucci, B., Petersson, G. A., Nakatsuji, H., Caricato, M., Li, X., Hratchian, H. P., Izmaylov, A. F., Bloino, J., Zheng, G., Sonnenberg, J. L., Hada, M., Ehara, M., Toyota, K., Fukuda, R., Hasegawa, J., Ishida, M., Nakajima, T., Honda, Y., Kitao, O., Nakai, H., Vreven, T., Montgomery, J. J. A., Peralta, J. E., Ogliaro, F., Bearpark, M., Heyd, J. J., Brothers, E., Kudin, K. N., Staroverov, V. N., Kobayashi, R., Normand, J., Raghavachari, K., Rendell, A., Burant, J. C., Iyengar, S. S., Tomasi, J., Cossi, M., Rega, N., Millam, J. M., Klene, M., Knox, J. E., Cross, J. B., Bakken, V., Adamo, C., Jaramillo, J., Gomperts, R., Stratmann, R. E., Yazyev, O., Austin, A. J., Cammi, R., Pomelli, C., Ochterski, J. W., Martin, R. L., Morokuma, K., Zakrzewski, V. G., Voth, G. A., Salvador, P., Dannenberg, J. J., Dapprich, S., Daniels, A. D., Farkas, O., Foresman, J. B., Ortiz, J. V., Cioslowski, J., and Fox, D. J.: Gaussian 09, Wallingford CT, 2009.

Gagné, S., Nieminen, T., Kurtén, T., Manninen, H. E., Petäjä, T., Laakso, L., Kerminen, V.-M., Boy, M., and Kulmala, M.: Factors influencing the contribution of ion-induced nucleation in

a boreal forest, Finland, Atmos. Chem. Phys., 10, 3743–3757, doi:10.5194/acp-10-3743-2010, 2010.

Galloway, M. M., Chhabra, P. S., Chan, A. W. H., Surratt, J. D., Flagan, R. C., Seinfeld, J. H., and Keutsch, F. N.: Glyoxal uptake on ammonium sulphate seed aerosol: reaction products and reversibility of uptake under dark and irradiated conditions, Atmos. Chem. Phys., 9, 3331–3345, doi:10.5194/acp-9-3331-2009, 2009.

Hanson, D. R. and Lovejoy, E. R.: Measurement of the thermodynamics of the hydrated dimer and trimer of sulfuric acid, J. Phys. Chem. A, 110, 9525–9528, doi:10.1021/Jp062844w, 2006.

Hari, P. and Kulmala, M.: Station for measuring ecosystem-atmosphere relations (SMEAR II), Boreal Env. Res., 10, 315–322, 2005.

Harrison, R. G. and Carslaw, K. S.: Ion-aerosol-cloud processes in the lower atmosphere, Rev. Geophys., 41, 1012, 26 pp., doi:10.1029/2002rg000114, 2003.

Heald, C. L., Kroll, J. H., Jimenez, J. L., Docherty, K. S., DeCarlo, P. F., Aikin, A. C., Chen, Q., Martin, S. T., Farmer, D. K., and Artaxo, P.: A simplified description of the evolution of organic aerosol composition in the atmosphere, Geophys. Res. Lett., 37, L08803, doi:10.1029/2010GL042737, 2010.

Hõrrak, U., Salm, J., and Tammet, H.: Diurnal variation in the concentration of air ions of different mobility classes in a rural area, J. Geophys. Res. A., 109(108),4653, 11 pp., doi:10.1029/2002jd003240, 2003.

Hõrrak, U., Aalto, P. P., Salm, J., Komsaare, K., Tammet, H., Mäkelä, J. M., Laakso, L., and Kulmala, M.: Variation and balance of positive air ion concentrations in a boreal forest, Atmos. Chem. Phys., 8, 655–675, doi:10.5194/acp-8-655-2008, 2008.

Hughey, C. A., Hendrickson, C. L., Rodgers, R. P., Marshall, A. G., and Qian, K. N.: Kendrick mass defect spectrum: A compact visual analysis for ultrahigh-resolution broadband mass spectra, Anal. Chem., 73, 4676–4681, 2001.

Junninen, H., Ehn, M., Petäjä, T., Luosujärvi, L., Kotiaho, T., Kostiainen, R., Rohner, U., Gonin, M., Fuhrer, K., Kulmala, M., and Worsnop, D. R.: A high-resolution mass spectrometer to measure atmospheric ion composition, Atmos. Meas. Tech., 3, 1039–1053, doi:10.5194/amt-3-1039-2010, 2010.

Kazil, J. and Lovejoy, E. R.: Tropospheric ionization and aerosol production: A model study, J. Geophys. Res. A., 109, D19206, doi:10.1029/2004jd004852, 2004.

Kazil, J., Harrison, R. G., and Lovejoy, E. R.: Tropospheric new particle formation and the role of ions, Space Sci. Rev., 137, 241–255, doi:10.1007/s11214-008-9388-2, 2008.

Kendrick, E.: A mass scale based on $CH_2=14.0000$ for high resolution mass spectrometry of organic compounds, Anal. Chem., 35, 2146–2154, 1963.

Kerminen, V.-M., Petäjä, T., Manninen, H. E., Paasonen, P., Nieminen, T., Sipilä, M., Junninen, H., Ehn, M., Gagné, S., Laakso, L., Riipinen, I., Vehkamäki, H., Kurten, T., Ortega, I. K., Dal Maso, M., Brus, D., Hyvärinen, A., Lihavainen, H., Leppä, J., Lehtinen, K. E. J., Mirme, A., Mirme, S., Hõrrak, U., Berndt, T., Stratmann, F., Birmili, W., Wiedensohler, A., Metzger, A., Dommen, J., Baltensperger, U., Kiendler-Scharr, A., Mentel, T. F., Wildt, J., Winkler, P. M., Wagner, P. E., Petzold, A., Minikin, A., Plass-Dülmer, C., Pöschl, U., Laaksonen, A., and Kulmala, M.: Atmospheric nucleation: highlights of the EUCAARI project and future directions, Atmos. Chem. Phys. Discuss., 10, 16497–16549,

doi:10.5194/acpd-10-16497-2010, 2010.

Kerminen, V. M., Anttila, T., Petäjä, T., Laakso, L., Gagné, S., Lehtinen, K. E. J., and Kulmala, M.: Charging state of the atmospheric nucleation mode: Implications for separating neutral and ion-induced nucleation, J. Geophys. Res. A., 109(112), D21205, doi:10.1029/2007jd008649, 2007.

Kroll, J. H., Donahue, N. M., Jimenez J. L., Kessler, S. H., Cangaratna, M. R., Wilson, K. R., Smith, J. D., Bluhm, H., Mysak, E. R., Kolb, C. E., and Worsnop, D. R.: Carbon Oxidation State and the Chemistry of Atmospheric Organic Aerosol, in preparation, 2010.

Ku, B. K. and de la Mora, J. F.: Relation between electrical mobility, mass, and size for nanodrops 1–6.5 nm in diameter in air, Aerosol Sci. Tech., 43, 241–249, doi:10.1080/02786820802590510, 2009.

Kulmala, M., Vehkamäki, H., Petäjä, T., Dal Maso, M., Lauri, A., Kerminen, V.-M., Birmili, W., and McMurry, P. H.: Formation and growth rates of ultrafine atmospheric particles: a review of observations, J. Aerosol Sci., 35, 143–176, 2004.

Kulmala, M., Lehtinen, K. E. J., and Laaksonen, A.: Cluster activation theory as an explanation of the linear dependence between formation rate of 3nm particles and sulphuric acid concentration, Atmos. Chem. Phys., 6, 787–793, doi:10.5194/acp-6-787-2006, 2006.

Kulmala, M., Riipinen, I., Sipilä, M., Manninen, H. E., Petäjä, T., Junninen, H., Dal Maso, M., Mordas, G., Mirme, A., Vana, M., Hirsikko, A., Laakso, L., Harrison, R. M., Hanson, I., Leung, C., Lehtinen, K. E. J., and Kerminen, V. M.: Toward direct measurement of atmospheric nucleation, Science, 318, 89–92, doi:10.1126/science.1144124, 2007.

Kulmala, M. and Kerminen, V. M.: On the formation and growth of atmospheric nanoparticles, Atmos. Res., 90, 132–150, doi.10.1016/j.atmosres.2008.01.005, 2008.

Kulmala, M., Asmi, A., Lappalainen, H. K., Carslaw, K. S., Poschl, U., Baltensperger, U., Hov, O., Brenguier, J. L., Pandis, S. N., Facchini, M. C., Hansson, H. C., Wiedensohler, A., and O'Dowd, C. D.: Introduction: European Integrated Project on Aerosol Cloud Climate and Air Quality interactions (EUCAARI) – integrating aerosol research from nano to global scales, Atmos. Chem. Phys., 9, 2825–2841, doi:10.5194/acp-9-2825-2009, 2009.

Kulmala, M., Riipinen, I., Nieminen, T., Hulkkonen, M., Sogacheva, L., Manninen, H. E., Paasonen, P., Petäjä, T., Dal Maso, M., Aalto, P. P., Viljanen, A., Usoskin, I., Vainio, R., Mirme, S., Mirme, A., Minikin, A., Petzold, A., Hõrrak, U., Plaß-Dülmer, C., Birmili, W., and Kerminen, V.-M.: Atmospheric data over a solar cycle: no connection between galactic cosmic rays and new particle formation, Atmos. Chem. Phys., 10, 1885–1898, doi:10.5194/acp-10-1885-2010, 2010.

Kumar, M. R., Prabhakar, S., Nagaveni, V., and Vairamani, M.: Estimation of gas-phase acidities of a series of dicarboxylic acids by the kinetic method, Rapid Communications in Mass Spectrometry, 19, 1053–1057, doi:10.1002/Rcm.1888, 2005.

Kurtén, T., Noppel, M., Vehkamäki, H., Salonen, M., and Kulmala, M.: Quantum chemical studies of hydrate formation of H_2SO_4 and HSO_4, Boreal Env. Res., 12, 431–453, 2007.

Kurtén, T., Berndt, T., and Stratmann, F.: Hydration increases the lifetime of HSO_5 and enhances its ability to act as a nucleation precursor – a computational study, Atmos. Chem. Phys.,

9, 3357–3369, doi:10.5194/acp-9-3357-2009, 2009.

Laakso, L., Gagné, S., Petäjä, T., Hirsikko, A., Aalto, P. P., Kulmala, M., and Kerminen, V.-M.: Detecting charging state of ultra-fine particles: instrumental development and ambient measurements, Atmos. Chem. Phys., 7, 1333–1345, doi:10.5194/acp-7-1333-2007, 2007.

Laakso, L., Laakso, H., Aalto, P. P., Keronen, P., Petäjä, T., Nieminen, T., Pohja, T., Siivola, E., Kulmala, M., Kgabi, N., Molefe, M., Mabaso, D., Phalatse, D., Pienaar, K., and Kerminen, V.-M.: Basic characteristics of atmospheric particles, trace gases and meteorology in a relatively clean Southern African Savannah environment, Atmos. Chem. Phys., 8, 4823–4839, doi:10.5194/acp-8-4823-2008, 2008.

Loukonen, V., Kurtén, T., Ortega, I. K., Vehkamäki, H., Pádua, A. A. H., Sellegri, K., and Kulmala, M.: Enhancing effect of dimethylamine in sulfuric acid nucleation in the presence of water – a computational study, Atmos. Chem. Phys., 10, 4961–4974, doi:10.5194/acp-10-4961-2010, 2010.

Manninen, H., Nieminen, T., and Asmi, E., Gagné, S., Häkkinen, S., Vana, M., Mirme, A., Mirme, S., Hõrrak, U., Plaß-Dülmer, C., Stange, G., Kiss, G., Hoffer, A., Moerman, M., Henzing, B., Brinkenberg, M., Kouvarakis, G.N., Bougiatioti, K., O'Dowd, C.D., Ceburnis, D., Svenningsson, B., Swietlicki, E., Tarozzi, L., Decesari, S., Sonntag, A., Birmili, W., Wiedensohler, A., Boulon, J., Sellegri, K., Laj, P., Baltensperger, U., Joutsensaari, J., Petäjä, T., Kerminen, V.-M., and Kulmala, M.: Initial steps of particle formation and growth in various environments during EUCAARI project, Atmos. Chem. Phys. Discuss., in preparation, 2010.

Manninen, H. E., Nieminen, T., Riipinen, I., Yli-Juuti, T., Gagné, S., Asmi, E., Aalto, P. P., Petäjä, T., Kerminen, V.-M., and Kulmala, M.: Charged and total particle formation and growth rates during EUCAARI 2007 campaign in Hyytil, Atmos. Chem. Phys., 9, 4077–4089, doi:10.5194/acp-9-4077-2009, 2009a.

Manninen, H. E., Petäjä, T., Asmi, E., Riipinen, I., Nieminen, T., Mikkilä, J., Hõrrak, U., Mirme, A., Mirme, S., Laakso, L., Kerminen, V. M., and Kulmala, M.: Long-term field measurements of charged and neutral clusters using Neutral cluster and Air Ion Spectrometer (NAIS), Boreal Env. Res., 14, 591–605, 2009b.

Mavri, J. and Hadzi, D.: Influence of solvation on the hydrogen bond in hydrogen malonate – An ab initio and semiempirical study, Journal of Molecular Structure-Theochem, 432, 257–262, 1998.

Merikanto, J., Spracklen, D. V., Mann, G. W., Pickering, S. J., and Carslaw, K. S.: Impact of nucleation on global CCN, Atmos. Chem. Phys., 9, 8601–8616, doi:10.5194/acp-9-8601-2009, 2009.

Mirme, A., Tamm, E., Mordas, G., Vana, M., Uin, J., Mirme, S., Bernotas, T., Laakso, L., Hirsikko, A., and Kulmala, M.: A wide-range multi-channel air ion spectrometer, Boreal Env. Res., 12, 247–264, 2007.

Mirme, S., Mirme, A., Minikin, A., Petzold, A., Hõrrak, U., Kerminen, V.-M., and Kulmala, M.: Atmospheric sub-3 nm particles at high altitudes, Atmos. Chem. Phys., 10, 437–451, doi:10.5194/acp-10-437-2010, 2010.

Montgomery, J. A., Frisch, M. J., Ochterski, J. W., and Petersson, G. A.: A complete basis set model chemistry. VI. Use of density functional geometries and frequencies, J. Chem. Phys., 110, 2822–2827, 1999.

Montgomery, J. A., Frisch, M. J., Ochterski, J. W., and Petersson, G. A.: A complete basis set model chemistry. VII. Use of the minimum population localization method, J. Chem. Phys., 112, 6532–6542, 2000.

Ortega, I. K., Kurtén, T., Vehkamäki, H., and Kulmala, M.: The role of ammonia in sulfuric acid ion induced nucleation, Atmos. Chem. Phys., 8, 2859–2867, doi:10.5194/acp-8-2859-2008, 2008.

Petäjä, T., Mauldin, III, R. L., Kosciuch, E., McGrath, J., Nieminen, T., Paasonen, P., Boy, M., Adamov, A., Kotiaho, T., and Kulmala, M.: Sulfuric acid and OH concentrations in a boreal forest site, Atmos. Chem. Phys., 9, 7435–7448, doi:10.5194/acp-9-7435-2009, 2009.

Salcedo, D., Villalta, P. W., Varutbangkul, V., Wormhoudt, J. C., Miake-Lye, R. C., Worsnop, D. R., Ballenthin, J. O., Thorn, W. F., Viggiano, A. A., Miller, T. M., Flagan, R. C., and Seinfeld, J. H.: Effect of relative humidity on the detection of sulfur dioxide and sulfuric acid using a chemical ionization mass spectrometer, Int. J. Mass Spectrom., 231, 17–30, doi:10.1016/j.ijms.2003.09.005, 2004.

Sipilä, M., Berndt, T., Petäjä, T., Brus, D., Vanhanen, J., Stratmann, F., Patokoski, J., Mauldin, R. L., Hyvärinen, A. P., Lihavainen, H., and Kulmala, M.: The role of sulfuric acid in atmospheric nucleation, Science, 327, 1243–1246, doi:10.1126/science.1180315, 2010.

Smith, J., Barsanti, K., Friedli, H., Ehn, M., Kulmala, M., Collins, D., Scheckman, J., Williams, B., and McMurry, P.: Observations of aminium salts in atmospheric nanoparticles and possible climatic implications, P. Natl. Acad. Sci., 107, 6634-6639, doi:10.1073/pnas.0912127107, 2009.

Suni, T., Kulmala, M., Hirsikko, A., Bergman, T., Laakso, L., Aalto, P. P., Leuning, R., Cleugh, H., Zegelin, S., Hughes, D., van Gorsel, E., Kitchen, M., Vana, M., Hõrrak, U., Mirme, S., Mirme, A., Sevanto, S., Twining, J., and Tadros, C.: Formation and characteristics of ions and charged aerosol particles in a native Australian Eucalypt forest, Atmos. Chem. Phys., 8, 129–139, doi:10.5194/acp-8-129-2008, 2008.

Tammet, H.: Continuous scanning of the mobility and size distribution of charged clusters and nanometer particles in atmospheric air and the Balanced Scanning Mobility Analyzer BSMA, Atmos. Res., 82, 523–535, doi:10.1016/j.atmosres.2006.02.009, 2006.

Vana, M., Ehn, M., Petäjä, T., Vuollekoski, H., Aalto, P., de Leeuw, G., Ceburnis, D., O'Dowd, C. D., and Kulmala, M.: Characteristic features of air ions at Mace Head on the west coast of Ireland, Atmos. Res., 90, 278–286, doi:10.1016/j.atmosres.2008.04.007, 2008.

Wang, M. and Penner, J. E.: Aerosol indirect forcing in a global model with particle nucleation, Atmos. Chem. Phys., 9, 239–260, doi:10.5194/acp-9-239-2009, 2009.

Wang, X. B., Nicholas, J. B., and Wang, L. S.: Photoelectron spectroscopy and theoretical calculations of SO4- and HSO4-: Confirmation of high electron affinities of SO_4 and HSO_4, J. Phys. Chem. A, 104, 504–508, 2000.

Weber, R. J., Marti, J. J., McMurry, P. H., Eisele, F. L., Tanner, D. J., and Jefferson, A.: Measurements of new particle formation and ultrafine particle growth rates at a clean continental site, J. Geophys. Res. A, 102, 4375–4385, 1997.

Yu, F. and Turco, R. P.: From molecular clusters to nanoparticles: Role of ambient ionization in tropospheric aerosol formation, J. Geophys. Res., 106, 4797–4814, 2001.

Yu, F., Wang, Z., Luo, G., and Turco, R.: Ion-mediated nucleation as an important global source of tropospheric aerosols, Atmos. Chem. Phys., 8, 2537–2554, doi:10.5194/acp-8-2537-2008, 2008.